[4] W. A. Harrison, *Solid State Theory*. New York: McGraw-Hill, 1970, pp. 280–290.
[5] R. J. Batt, G. D. Jones, and D. J. Harris, "The Measurement of the surface resistivity of evaporated gold at 890 GHz," *IEEE Trans. Microwave Theory Tech.*, vol. MTT-25, pp. 488–491, June 1977.
[6] R. Kubo and T. Nagamiya, Eds., *Solid State Physics*. New York: McGraw-Hill, 1969, pp. 245–249.
[7] A. A. Abrikosov, *Introduction to The Theory of Normal Metals, Solid State Physics*, H. Ehrenreich, F. Seitz, and D. Turnball, Eds., Suppl. 12. New York: Academic, 1972, ch. 5.
[8] F. Wooten, *Optical Properties of Solids*. New York: Academic, 1972, ch. 4.

The Traveling-Wave IMPATT Mode

MICHAEL FRANZ AND JAMES B. BEYER, MEMBER, IEEE

Abstract—**The small-signal analysis of a distributed IMPATT diode ifdicates the existence of a traveling-wave mode. The severe power-frequency limitation as well as the associated low impedance level of the discrete diode appear avoidable. No external resonant circuitry is needed.**

It is shown that the TEM parallel-plate waveguide mode of the junction is modified by the injection of electrons at the p^+-n junction (or Schottky contact). The transverse electric field takes on a traveling-wave nature in the transverse direction tracking the injected electrons, and a small longitudinal electric field will also be present.

In previous papers on IMPATT traveling-wave structures, the IMPATT effect was lumped into an effective complex permittivity in a composite layer model or into an effective shunt admittance in a transmission line model. The current work attempts to incorporate the IMPATT mechanism into the wave model and considers the actual carrier field interaction.

The small-signal analysis yields an analytic field solution and a characteristic equation for the complex propagation constant. Solutions are found and documented for various frequencies and bias current densities. For the particular structure considered, at 12 GHz with a bias current density of 1000 A/cm^2 a gain of 72 dB/cm was found.

I. Introduction

THE QUANTITATIVE model of traveling-wave behavior in an IMPATT diode is based on the idealized structure of Fig. 1. The diode shown is essentially an IMPATT diode elongated in the z direction, wherein the p^+-n^+-n sandwich of the diode is contacted by two metallic layers.

Due to the distributed nature of the device, the power-frequency limitation associated with a lumped diode will not apply with the additional advantage that no external resonant circuitry is needed, which points to the possibility of direct integration. The application of the diode as an amplifier, modulator (phase shifter), or as an oscillator would depend on the coupling and matching scheme used.

To obtain a qualitative understanding of the traveling-wave behavior, it is assumed that the diode of Fig. 1 is reversed biased and that a TEM parallel-plate waveguide mode exists in the depletion layer. Neglecting fringing effects, the electric ac field will be given by

$$E_x = E_0 e^{\gamma z} \tag{1}$$

with γ as the wavenumber.

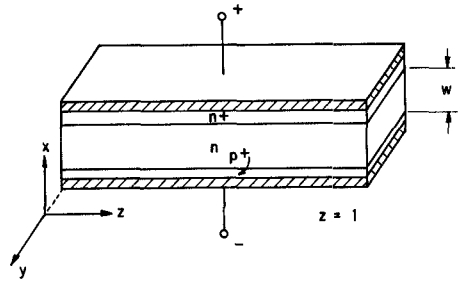

Fig. 1. Distributed IMPATT diode.

An instantaneous picture of E_x is shown in Fig. 2(a). In IMPATT operation, the avalanche carrier built up at the p^+-n junction will reach its maximum after the completion of the negative half-cycle. At the transit time frequency

$$f = \frac{v_s}{2w} \tag{2}$$

the electrons cross the depletion region with scattering limited velocity during the positive half-cycle and are collected by the n^+ substrate. The front of maximum electron density is symbolized in Fig. 2(b) for a wave traveling to the right. The traversing electrons constitute a current opposing the ac electric field and contribute RF power to the wave.

Thus the principles of power transfer in the distributed diode from a dc source to an RF signal are the same as those in the lumped diode, only here the IMPATT process propagates with the wave. These principles can be summarized as follows.

1) In the depletion region of the diode, power is added to an existing RF electric field by forcing charge carriers

Manuscript received December 9, 1977; revised March 23, 1978.
The authors are with the Department of Electrical and Computer Engineering, University of Wisconsin-Madison, Madison, WI 53706.

0018-9480/78/1100-0861$00.75 ©1978 IEEE

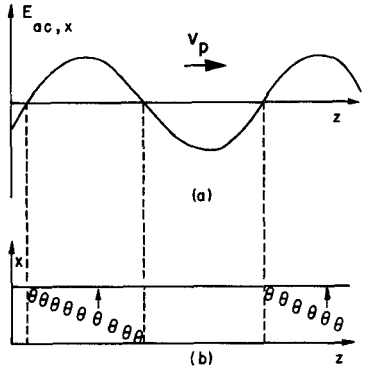

Fig. 2. (a) Instantaneous picture of the ac electric field. (b) Electrons symbolize maximum density of carriers traveling across space charge region.

to move through the RF field against the associated coulomb force qE_{RF}.

2) The external force driving the charge carriers against the RF field is provided by the dc electric field.

3) A timing mechanism is needed, which results in charge carriers moving through the depletion region during the half-cycle with positive RF power gain, i.e., while the RF electric field opposes the carrier motion. This mechanism is provided by the avalanche carrier multiplication and the carrier transit time.

Several authors treated an IMPATT traveling-wave diode. Midford and Bowers [1] actually built a distributed diode. A transmission line model with negative shunt conductance is mentioned, but no analysis is shown. The measurements indicate RF gain and traveling-wave behavior, both being functions of the bias current. In a paper by Davydova, Danyushevsky, and Telyatnikov [2], the theoretical analysis is performed based on a transmission line model. The results are in qualitative agreement with the findings in [1]. By far the most elaborate treatment so far was presented by Hambleton and Robson [3], who analyzed a composite parallel-plate waveguide structure where the IMPATT mechanism is modeled by an effective negative conductivity in the depletion layer.

The current paper is an attempt to analyze an IMPATT traveling-wave amplifier by actually considering the interaction of avalanche triggered carriers with the electric field rather than lumping all IMPATT effects into an effective conductance or conductivity. The analysis indeed shows that current density and electric field cannot be related by a complex *constant* throughout the depletion region.

The small-signal model of an IMPATT traveling-wave structure is developed. Gain and dispersion relationship of possible waves are displayed graphically for a particular device.

II. Mathematical Model

The analysis of the previously described structure is based on six equations.

1) Gauss' law as applied to the space charge region with donor ions and electrons as charges

$$\nabla\cdot\bar{E}=\frac{q}{\epsilon}(N_D-n). \tag{3}$$

2) The wave equation for the E field from Maxwell's first and second equations

$$\nabla^2\bar{E}-\nabla(\nabla\cdot\bar{E})-\mu\epsilon\frac{\partial^2\bar{E}}{\partial t^2}-\mu\frac{\partial\bar{J}_c}{\partial t}=0 \tag{4}$$

where $\bar{J}_c$ is the conduction current density.

3) Boundary conditions on E

$$E_z(x=0)=E_z(x=w)=0 \tag{5}$$

i.e., the highly doped p^+ and n^+ regions are approximated by perfect conductors.

4) Avalanche carrier generation governed by

$$\frac{\tau_1}{2}\frac{\partial J_0}{\partial t}=J_0\left(\int_0^{x_1}\alpha(E)\,dx-1\right)+J_s \tag{6}$$

where

x_1	width of avalanche region,
α	ionization constant,
J_s	saturation current density,
$\tau_1=x_1/v_s$	avalanche region transit time,
$J_0=-qv_sn$	electron current density at x_1.

5) Carrier transport

$$n(x,z,t)=n\left(0,z,t-\frac{x}{v_s}\right) \tag{7}$$

wherein it has been assumed that the injected electrons drift undispersed across the space charge region with scattering limited velocity v_s.

6) Conduction current density given by

$$\bar{J}_c=-qv_sn\hat{a}_x \tag{8}$$

with diffusion currents in the x and z direction neglected. $\hat{a}_x$ is the unit vector in x direction.

Using $J_0=-qv_sn$ in (6) and assuming a dependence of the ionization constant $\alpha\sim E^m$, the integration in the avalanche zone can be performed [4] resulting in

$$\frac{\partial n(x=0)}{\partial t}=\frac{2}{\tau_1}n(x=0)\left[\left(\frac{E(x=0)}{E_c}\right)^{m+1}-1\right]-\frac{2}{\tau_1qv_s}J_s \tag{9}$$

where E_c is the critical field at breakdown at $x=0$. This set of six equations is now rewritten in terms of a two-dimensional model, and E_z is eliminated.

$$\nabla^2E_x-\mu\epsilon\frac{\partial^2E_x}{\partial t^2}=\frac{q}{\epsilon}\frac{\partial}{\partial x}(N_D-n)-\mu qv_s\frac{\partial n}{\partial t} \tag{10}$$

$$\frac{\partial E_x}{\partial x}\left(\begin{matrix}x=0\\x=w\end{matrix}\right)=\frac{q}{\epsilon}\left[N_D\left(\begin{matrix}x=0\\x=w\end{matrix}\right)-n\left(\begin{matrix}x=0\\x=w\end{matrix}\right)\right] \tag{11}$$

$$\frac{\partial n}{\partial t}(x=0)=\frac{2}{\tau_1}n(x=0)\left[\left(\frac{E_x(x=0)}{E_c}\right)^{m+1}-1\right]-\frac{2}{\tau_1qv_s}J_s \tag{12}$$

$$n(x,z,t)=n\left(0,z,t-\frac{x}{v_s}\right). \tag{13}$$

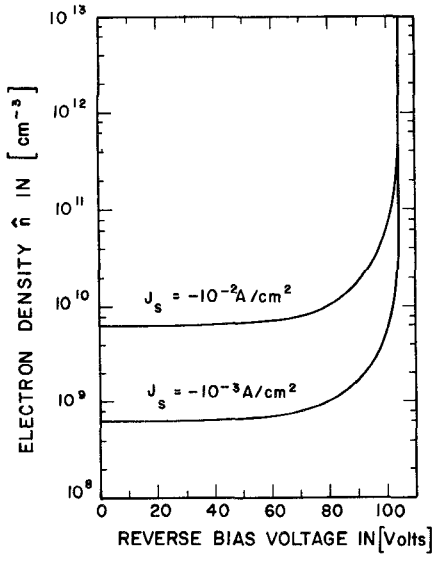

Fig. 3. DC electron density $\hat{n}$ versus reverse biased voltage for two saturation current densities.

For the small-signal analysis, E_x and n are split into a time average and time harmonic component.

$$E_x(x,z,t)=\hat{E}_x(x,z)+\tilde{E}_x(x,z)e^{j\omega t} \tag{14}$$

$$n(x,z,t)=\hat{n}(x,z)+\tilde{n}(x,z)e^{j\omega t}. \tag{15}$$

The equation system (10) through (13) separates into a dc and an ac part. The solution of the dc system is straightforward and omitted here; the only important result for the later ac treatment is that $\hat{n}(x,z)$ turns out to be a constant, the value of which can be arbitrarily set by the externally applied bias current or voltage as suggested by Fig. 3.

III. AC System

Ignoring higher harmonics of the nonlinear equation (12), the ac small-signal equation system becomes

$$\frac{\partial^2\tilde{E}_x}{\partial x^2}+\frac{\partial^2\tilde{E}_s}{\partial z^2}+\omega^2\mu\epsilon\tilde{E}_x=-\frac{q}{\epsilon}\frac{\partial\tilde{n}}{\partial x}-j\omega\mu q v_s\tilde{n} \tag{16}$$

$$\frac{\partial\tilde{E}_x}{\partial x}\begin{pmatrix}x=0\\x=w\end{pmatrix}=-\frac{q}{\epsilon}\tilde{n}\begin{pmatrix}x=0\\x=w\end{pmatrix} \tag{17}$$

$$\tilde{n}(x=0)=\frac{2(m+1)\hat{n}}{j\omega\tau_1 E_C}\tilde{E}_x(0) \tag{18}$$

$$\tilde{n}(x,z)=\tilde{n}(0,z)e^{-j\frac{\omega}{v_s}x} \tag{19}$$

where the assumption was made in (18) that $\hat{E}_x(0)\cong E_c$.

Our interest centers on traveling waves in the z direction. By eliminating $\tilde{n}(x,z)$ by means of (18), (19) and looking specifically for a traveling-wave solution of the form

$$\tilde{E}_x(x,z)=\mathring{E}_x(x)e^{\gamma z} \tag{20}$$

an ordinary linear inhomogeneous differential equation with homogeneous boundary conditions is obtained; an eigenvalue problem in γ:

$$\frac{d^2\mathring{E}_x}{dx^2}+(\gamma^2+\omega^2\mu\epsilon)\mathring{E}_x=\frac{2q(m+1)\hat{n}\mathring{E}_x(0)}{\tau_1 E_C}\cdot\left(\frac{1}{\epsilon v_s}-\mu v_s\right)e^{-j(\omega/v_s)x} \tag{21}$$

$$\frac{d\mathring{E}_x}{dx}(0)=-\frac{2q(m+1)\hat{n}}{j\omega\epsilon\tau_1 E_c}\mathring{E}_x(0) \tag{22}$$

$$\frac{d\mathring{E}_x}{dx}(w)=-\frac{2q(m+1)\hat{n}}{j\omega\epsilon\tau_1 E_c}\mathring{E}_x(0)e^{-j(\omega/v_s)w}. \tag{23}$$

The problem now consists of the determination of the eigenvalues γ and the eigenvector $\mathring{E}_x(x)$.

For the ease of later computations, the x coordinate is normalized by the length v_s/ω such that

$$x_n=\frac{x}{(v_s/\omega)} \tag{24}$$

and a set of new parameters is introduced.

$$\frac{\partial^2\mathring{E}_x}{\partial x_n^2}+a_n^2\mathring{E}_x=gf\mathring{E}_x(0)e^{-jx_n} \tag{25}$$

$$\frac{\partial\mathring{E}_x}{\partial x}(0)=jg\mathring{E}_x(0) \tag{26}$$

$$\frac{\partial\mathring{E}_x}{\partial x}(w_n)=jge^{-jw_n}\mathring{E}_x(0) \tag{27}$$

where

$$a_n^2=(\gamma^2+\omega^2\mu\epsilon)\frac{v_s^2}{\omega^2} \tag{28}$$

$$g=\frac{2\hat{n}(m+1)qv_s}{\omega^2\tau_1 E_c} \tag{29}$$

$$c^2=\epsilon\mu v_s^2 \tag{30}$$

$$f=1-c^2. \tag{31}$$

The general solution of (25) is of the form

$$\mathring{E}_x(x_n)=Ae^{ja_nx_n}+Be^{-ja_nx_n}+\frac{gf\mathring{E}_x(0)e^{-jx_n}}{a_n^2-1},\qquad a_n^2\neq 1. \tag{32}$$

The two boundary conditions (26) and (27) plus the condition that $\mathring{E}_x(x_n)$ must be self-consistent at $x_n=0$ can be expressed in matrix form

$$\begin{bmatrix}1 & 1 & \left(\frac{gf}{a_n^2-1}-1\right)\\ a_n & -a_n & -g\left(\frac{f}{a_n^2-1}+1\right)\\ a_ne^{ja_nw_n} & -a_ne^{-ja_nw_n} & -g\left(\frac{f}{a_n^2-1}+1\right)e^{-jw_n}\end{bmatrix}\begin{bmatrix}A\\B\\\mathring{E}_x(0)\end{bmatrix}=0. \tag{33}$$

The condition for the existence of a solution of (33) is that the determinant of the matrix be zero, resulting in the following characteristic equation:

$$a_n g\left(\frac{a_n^2-c^2}{a_n^2-1}\right)e^{-jw_n}-a_n g\left(\frac{a_n^2-c^2}{a_n^2-1}\right)\cos a_n w_n + ja_n^2\left(\frac{gf}{a_n^2-1}-1\right)\sin a_n w_n=0. \quad (34)$$

The trivial solution $a_n=0$ is readily identified as the dc case with $\dot{E}_x(x)\equiv 0$.

IV. Results

It is noted at this point that (34) reduces to the characteristic equation of a parallel-plate transmission line if the carrier injection is turned off (no bias current). Then $\hat{n}=0$ and $g=0$.

$$\sin a_n w_n=0. \quad (35)$$

For this case, the dispersion relation becomes with (28)

$$\gamma_n^2=\frac{n^2\pi^2}{w^2}-\omega^2\mu\epsilon, \qquad n=0,1,2,\cdots. \quad (36)$$

Thus with a depletion width $w=7\times10^{-4}$ cm and an $\epsilon_r=11.8$ for Si, the first cutoff frequency of the next higher mode $f_1\cong 6.2\times10^{12}$ Hz is far above the IMPATT transit time frequency $f_t=v_s/2w\cong 7$ GHz. The associated characteristic impedance is

$$Z_0\simeq\eta\frac{w}{b} \quad (37)$$

where η is the intrinsic impedance, and b is the width of metal contacts. For $b=10^{-2}$ cm and $\eta_{Si}=\sqrt{\mu_0/\epsilon}=109.7$ Ω, the impedance becomes $Z_0=7.7$ Ω.

For the more general case of carrier injection, the roots a_n of (34) were found numerically for various current densities and frequencies. The propagation constant of the fundamental mode is determined from (28) as

$$\gamma=\sqrt{a_n^2\frac{w^2}{v_s^2}-\omega^2\mu\epsilon}\ . \quad (38)$$

Fig. 4 is a plot of $\gamma=\alpha+j\beta$ in the complex plane for a particular diode.[1] It is recalled that the z dependence of the electric field was expressed in (20)

$$\tilde{E}_x(x,z)=\dot{E}(x)e^{\gamma z}. \quad (20)$$

Hence, for α and β having equal signs, the wave will be attenuated in the propagation direction (the time factor is $e^{+j\omega t}$), whereas opposite signs indicate amplification. In Fig. 4, the third quadrant implies attenuation and the fourth implies gain. The solid curves are loci of constant frequency while the dc current density $J_{dc}=qv_s\hat{n}$ is varied between 0 and 1000 A/cm^2. The dashed curves give the propagation constant for a fixed current density with frequency as a parameter. The graph predicts a wide frequency range of gain from 2 to 14 GHz with maximum gain at frequencies rising with the dc current density. For zero current density, the constant frequency curves intersect the zero gain line, and the propagation constant is just that of the parallel plate transmission line $\gamma=-j\omega\sqrt{\epsilon\mu}$. For dc current densities below 250 A/cm^2, the constant frequency curves indicate gain. In particular, the increase of gain is largest close to the transit time frequency (≅7 GHz), and no phase shift is introduced; whereas at lower frequencies, the gain increase with current becomes smaller. A drastic phase shift (or a change of phase constant β) is seen: the curves leave the zero gain line at decreasing angles. Above the transit time frequency, a similar effect is seen except that the angles are increasing. In terms of wavelength it can be said: for low current densities, β is increased below and decreased above the transit time frequency.

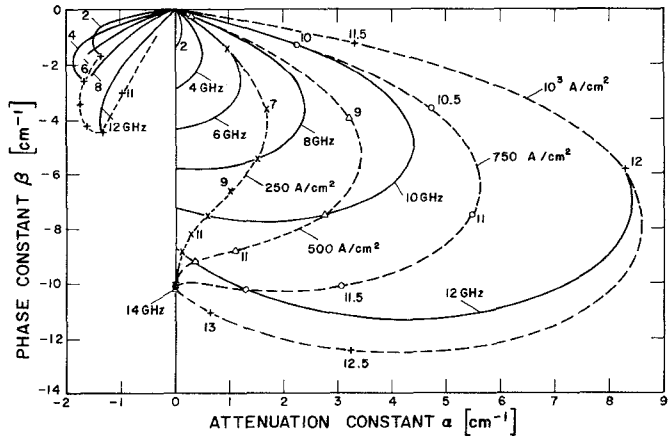

Fig. 4. Propagation constant $\gamma=\alpha+j\beta$; solid curves are constant frequency. Dashed curves are constant current loci.

If the current is increased further, the gain reaches its maximum after which it decreases and eventually turns into attenuation indicating an optimum carrier-field phase relation for each frequency. At 10^3 A/cm and 12 GHz, the graph predicts a gain of 72 dB in an 1-cm long line.

Fig. 5 shows the dispersion relationship. The development from a straight line for the TEM mode ($J_{dc}=0$) into curves of considerable dispersion is obvious. With the gain being the marker parameter, it is seen that maximum gain coincides with low group velocities, $v_g=\partial\omega/\partial\beta$. Slow waves with phase velocities $v_p=\omega/\beta$ below the intrinsic phase velocity $1/\sqrt{\epsilon\mu}$ are obtained to the right of the straight line.

In Fig. 6 the gain is plotted versus frequency. The increase of the maximum gain frequency with bias current follows essentially the square-root relation of the discrete diode $f_{max}\backsim\sqrt{J_{dc}}$. The active frequency band narrows for higher currents.

If we are actually interested in the electric ac field in the diode, A and B in (33) have to be evaluated in terms

[1]The particular diode considered had the following specifications. Material: Si; $\epsilon_r=11.8$; donor doping in depletion region $N_D=2.2\times10^{15}$cm^{-3}; depletion region width $w=7\mu$m; scattering limited veolocity $v_s=10^7$ cm/s; critical field $E_c=-2.66\times10^5$V/cm; and breakdown voltage $V_B=104$ V.

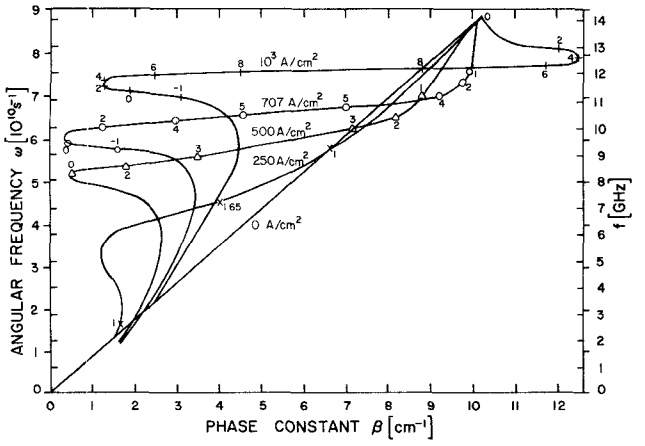

Fig. 5. Dispersion relationship ω versus β; gain α in Np/cm is marker parameter. DC current density J_{dc} is curve parameter.

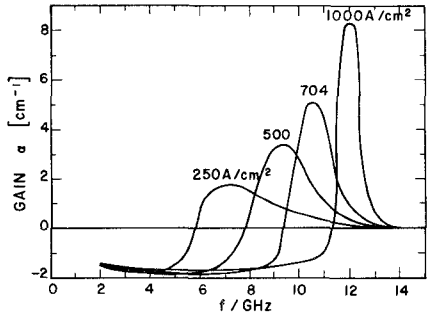

Fig. 6. Gain α versus frequency for various dc bias current densities J_{dc}.

of $\mathring{E}_x(0)$, and $\mathring{E}_x(x_n)$ is then given by (32). The z component of the electric field can then be obtained from Gauss' law

$$\frac{\partial \tilde{E}_z}{\partial z} = -\frac{q}{\epsilon}\tilde{n} - \frac{\partial \tilde{E}_x}{\partial x}. \tag{39}$$

The numerical evaluation of $\tilde{E}_z$ indicates that it is three to four orders of magnitude smaller than $\tilde{E}_x$ and hence can be ignored.

The magnitude and phase angle of $\mathring{E}_x$ are seen in Fig. 7 for a frequency $f = 12$ GHz and a current density of 10^3A/cm^2. The monotonically decreasing phase angle results from wave action in the x direction. The electric field is tracking the carrier wave. The dip of the magnitude of $\mathring{E}_x$ at $x \simeq 4$ μm can become much more pronounced for operation off the maximum gain frequency.

V. Conclusions

Small-signal analysis indicates the existence of an IMPATT traveling-wave mode. The mode system of a parallel-plate transmission line is modified by the avalanche timed injection of charge carriers. The fundamental mode was investigated, although the numerical

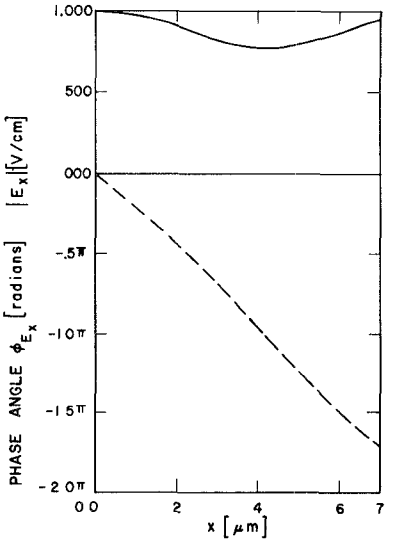

Fig. 7. Magnitude and phase angle (dashed curve) of E_x. Frequency $f = 12$ GHz. Current density $J_{dc} = 1000$ A/cm^2.

analysis indicated the presence of higher injection modes. Gain and wavelength can be influenced greatly by different bias current densities. For the device investigated, a maximum gain of 72 dB/cm was calculated at 12 GHz and a dc current density of 1000 A/cm^2. The electric field in the depletion region is essentially transverse. As seen from Fig. 7, the ac current density, constant in magnitude, is not relatable to the electric field by a complex constant. The traveling-wave nature of the electric field across the depletion region makes the concept of a characteristic impedance questionable. It seems it cannot be expressed simply by a voltage-to-current ratio of the incident wave, and matching conditions are still under investigation. The advantages of an IMPATT traveling-wave structure with respect to a lumped diode are as follows.

1) The beneficial use of the larger area for increased power gain.

2) The possibility of using the device without modification as an amplifier and/or modulator (phase shifter) or as an oscillator depending on the coupling and matching methods used.

3) The possibility of large-scale integration in solid-state devices without the need for external resonant circuitry.

References

[1] T. A. Midford and H. C. Bowers, "A two-port IMPATT diode traveling wave amplifier," *Proc. IEEE*, Oct. 1968.

[2] N. S. Davydova, Yu. Z. Danyushevsky, and L. I. Telyatnikov, "Linear theory of an IMPATT diode distributed microwave amplifier," *Telecommun. & Radio Eng., Pt. 2*, vol. 27, no. 8, pp. 112–115, Aug. 1972.

[3] K. G. Hambleton and P. N. Robson, "Design considerations for resonant traveling wave IMPATT oscillators," *Int. J. Electron.*, vol. 35, no. 2, pp. 225–244, 1973.

[4] S. M. Sze, *Physics of Semiconductor Devices*. New York: Wiley, 1969, pp. 215–221.